AGU PUBLICATIONS

JGR

Journal of Geophysical Research: Oceans

RESEARCH ARTICLE

10.1002/2016JC012511

Three-dimensional pathways of water masses in the South China Sea: A modeling study

Zhiqiang Liu[1] and Jianping Gan[1]

[1]Department of Mathematics & Division of Environment, Hong Kong University of Science and Technology, Clear Water Bay, Hong Kong

Key Points:
- The pathway of the SCS waters is determined not only by exchange with the neighboring oceans, but also by exchange between different layers
- The residence time (ReT) of SCS waters generally increases southward and downward, and the longest ReT (~42 years) exists in the intermediate layer
- The refreshment of deep waters in the basin is governed by an extensive cyclonic circulation in the southern South China Sea (south of 13°N)

Supporting Information:
- Supporting Information S1

Correspondence to:
J. Gan,
magan@ust.hk

Citation:
Liu, Z. and J. Gan (2017), Three-dimensional pathways of water masses in the South China Sea: A modeling study, *J. Geophys. Res. Oceans*, *122*, 6039–6054, doi:10.1002/2016JC012511.

Received 27 OCT 2016
Accepted 18 JUN 2017
Accepted article online 20 JUN 2017
Published online 28 JUL 2017

Abstract We conduct a numerical Eulerian analysis on the Lagrangian characteristics of South China Sea (SCS) water masses. This is the first study to investigate the water pathway and residence time in response to time-dependent, three-dimensional basin circulation in the SCS. The circulation of the SCS is largely determined by westward intrusions of the northwestern Pacific waters in the upper layer (0–750 m) and deep layer (>1500 m), and by an eastward extrusion in the intermediate layer (750–1500 m) through Luzon Strait (LS). The waters in these three layers are interlinked to sustain the three-dimensional circulation in the SCS. The upper intrusive waters flow cyclonically and have a residence time of ~3 years before they subduct into a deeper layer or exit the SCS through surrounding straits. The intrusive denser waters in the deep layer flow along the northern slope and reside for ~25 years in the northern basin (north of 13°N), where a strong subduction occurs. A cyclonic circulation exists in the deep layer in the southern basin (south of 13°N), where a subduction of intermediate waters occurs over its eastern side and a deep upwelling exists over its western side. The water in the deep southern basin has a residence time of ~40 years. The upwelled deep waters and the subducted waters from the upper layer form the intermediate water, where waters circulate anti-cyclonically toward LS and have a longest residence time (~42 years). These findings are supported by the spatial variation in the observed potential density variance.

1. Introduction

The South China Sea (SCS) is a semienclosed marginal sea in the tropical northwest Pacific Ocean (NPO, Figure 1a). Four restricted openings connect the SCS to surrounding oceans. The shallow (<100 m) Taiwan and Karimata Straits connect the northern (NSCS, north 13°N) and southern SCS (SSCS) to the East China Sea and Java Sea, respectively. The channels (<200 m) in the Palawan Archipelago join the southeastern SCS to the Sulu Sea, and the strongest water exchange in those channels occurs in Mindoro Strait (Figure 1b). Luzon Strait (LS), northeast of the SCS, is the deepest passage (~2500 m) connecting the SCS to the NPO.

The maximum water depth of the deep SCS basin is over 4000 m, and the basin is enclosed below 2500 m. Broad continental shelves sit on the western side of the NSCS and the SSCS. The central basin is surrounded by a semiclosed shelf slope between the 200 m and 3000 m isobaths. This slope has a complicated topography of seamounts and ridges northeast of Vietnam and bordering the Xisha Islands. There is a shallower basin, neighboring the Nansha Islands, in the SSCS, south of 9°N (Figure 1a). This closed basin, encircled by the 3000 m isobaths, is shaped like a rhombus, has a moderate slope, and is oriented northeastward.

Climatologically, the SCS circulation flows cyclonically along the surrounding slope [*Gan et al.*, 2016a]. We infer this flow pattern from the long-term (1993–2013) averaged absolute geostrophic velocity that is derived from satellite remote sensing provided by *Archiving, Validation, and Interpretation of Satellite Oceanographic Data* (AVISO) (Figure 1b). An extensive cyclonic circulation in the SCS basin is depicted. This circulation pattern originates from an intrusion of the Kuroshio Current (KC) into the upper layer through LS. The circulation weakens along its southwestward main stream over the slope in the NSCS. The main stream bifurcates near the Xisha Islands and forms a weaker southeastward branch. The main branch flows further southward along the slope, and intensifies over the narrow slope east of Vietnam. Part of this western boundary current (WBC) veers northeastward in the southernmost SSCS, converges with the southeastward branch from the Xisha Islands and exits the SCS through Mindoro Strait. The southward directed transport

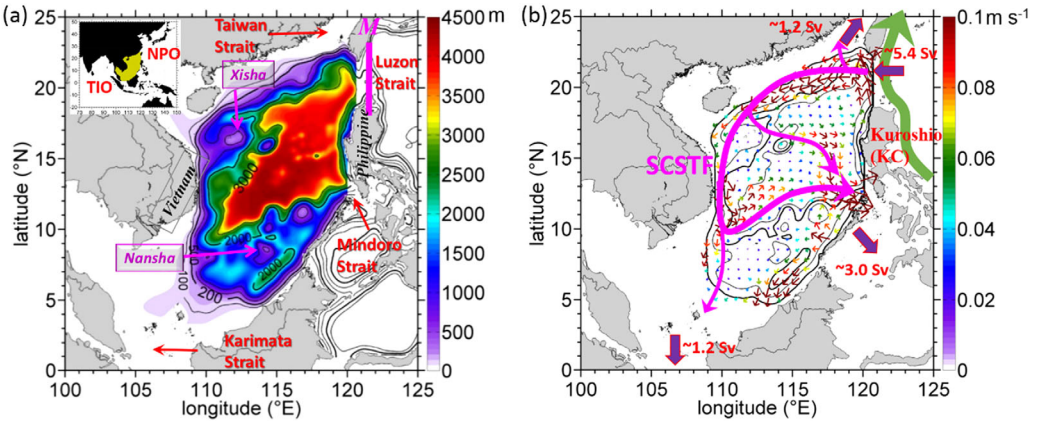

Figure 1. (a) Bathymetry in the SCS and (b) long-term (1993–2013) averaged absolute geostrophic velocity (m s^{-1}) vectors derived from satellite remote sensing of AVISO in the SCS. The volume transport in the straits surrounding the SCS is obtained from *Gan et al.* [2016a], and the 200, 1000, 2000, and 3000 m isobaths are shown in Figure 1b.

across the SCS basin is called the SCS Throughflow (SCSTF) [*Qu et al.*, 2006a]. It conveys the NPO waters through LS (Figure 1b) to the Java Sea, the East China Sea, and the Sulu Sea [*Qu et al.*, 2000].

The monsoon wind and the water intrusions/extrusions through the surrounding straits, especially in LS [*Gan et al.*, 2006, 2016a], jointly drive the SCSTF. Many studies have reported the existence of a three-layered exchanging flow through LS, and the associated three-layered circulation in the basin [*Xu and Oey*, 2014; *Gan et al.*, 2016a]. The NPO water, carried by the KC, branches westward in the upper layer of LS [*Wu and Hsin*, 2012], and, partly through the SCSTF, the NPO water communicates with the other surrounding oceans [*Fang et al.*, 2009]. A notable eastward outflow of SCS water is observed in the intermediate layer of LS [*Li and Qu*, 2006; *Gan et al.*, 2016b]. Thermal dynamics in the deep basin is regulated by an extensive intrusion of denser NPO water in the lower layer (1500–2500 m) of LS. The intrusive denser water sinks in the NSCS and imposes an energetic cyclonic circulation in the closed deep basin [*Lan et al.*, 2013]. There is extensive upwelling over the slope in the northwestern SCS and east of Vietnam to compensate for these subducted waters [*Chao et al.*, 1996]. The SCSTF is partly maintained by these upwelled denser waters [*Qu et al.*, 2009].

The subduction of the NPO water from the deep layer of LS refreshes the deep basin in approximately 100 years [*Broecker et al.*, 1986]. The strong deep inflow of about 1 Sv in the LS [*Zhou et al.*, 2014; *Gan et al.*, 2016a] and rapid deep water formation suggest a much shorter residence time (*ReT*) in the SCS than that in the neighboring NPO. Few studies have investigated the basin-scale pathway of the deep water, and the associated *ReT* of the water mass in the SCS remains largely unclear. The estimated *ReT* of the deep SCS water varies by an order magnitude of several decades [*Chou et al.*, 2007], and the spatial variation of *ReT* in the basin has never been documented. For example, *Qu et al.* [2006b] suggest that the SCS water below 1489 m is refreshed in 24 years. *Shu et al.* [2014] confirmed their estimate, based on the movement of Lagrangian tracers derived from the Hybrid Coordinate Ocean Model (HYCOM). *Yang et al.* [2012] is the only study that notes an increment in *ReT* with depth. They proposed that it takes ~48 years to form the intermediate and lower layers (850–3500 m), and that the *ReT* of the surface water is approximately 1.3 years. However, the three-dimensional variation in *ReT* and its connection with the pathway of the SCS waters have not been sufficiently investigated.

The pathway and *ReT* of water in a marginal sea usually exhibit remarkable spatial variation, and are closely characterized by the associated interior circulation and exterior exchanging flow. In this sense, the waters at different locations/depths of a vast basin, like SCS in this research, are controlled by the time-dependent, three-dimensional circulation, and have varying pathway and *ReT*. With the complex nature of the circulation, the residence time of water mass cannot be well presented by a flushing time, computed by dividing the volume of the basin with the exchanging flow along its boundary [e.g., *Yang et al.*, 2012]. It has long been realized that deep water is prone to be refreshed in the region/layer where cyclonic circulation prevails [*Gascard*, 1978]. For instance, the subduction of denser water in the northern half of the Red Sea forms the deep water and leads to a longer *ReT*, while its intermediate water has a much higher formation rate

due to the injection of warm saline water from the western Arabian Sea [*Sofianos and Johns*, 2015]. The Mediterranean Sea is another example of a marginal sea whose water pathways and *ReT* vary spatially [*Lascaratos et al*., 1999]. The deep water in the western Mediterranean Sea has a much longer *ReT* (~100 years) than the deep water in the eastern Mediterranean Sea (20–40 years). The deep water in the eastern Mediterranean, and the associated thermal dynamics, are modulated by subduction of intermediate water in the Adriatic and the Aegean Seas [*Gačić et al*., 2011].

We perform numerical Eulerian analysis on Lagrangian tracers to explore the pathways of the water masses in the semiclosed SCS. This paper is organized as follows. In section 2, we use the potential density variance derived from the World Ocean Atlas 2013 (WOA13) [*Zweng et al*., 2013] to explore the pathways of the SCS waters. The model implementation and dynamics configuration, and the general SCS circulation, are introduced in section 3. Section 4 presents a three-dimensional picture of *ReT* in the SCS. In section 5, we discuss the extrinsic controls from the NPO on the pathways of deep SCS water. We summarize our findings and draw conclusions in section 6.

2. Observed Characteristics of Water Pathways in the SCS

The observed characteristics of the SCS water pathways are derived from the climatological averages of the 0.25°×0.25° gridded potential density (ρ_θ). We calculate ρ_θ from the annually-averaged products of temperature and salinity available from the WOA13 data set. We deduct ρ_θ by using the horizontally averaged $\overline{\rho_\theta}$ in the SCS to retrieve the potential density variance ($\rho_\theta{}'$) at the WOA13 standard depths. Then, $\rho_\theta{}'$, at different locations (x, y, z) of the SCS, can be expressed as

$$\rho_\theta{}'(x,y,z)=\rho_\theta(x,y,z)-\frac{\int\int_{SCS}\rho_\theta(x,y,z)dxdy}{\int\int_{SCS}dxdy}, \tag{1}$$

where $\overline{\rho_\theta}(z)=\frac{\int\int_{SCS}\rho_\theta(x,y,z)dxdy}{\int\int_{SCS}dxdy}$, and $\rho_\theta{}'$ represents the density variation induced by the exchange and migration of seawater, especially in the water below the surface mixed layer (< 200 m) where the impact of evaporation and precipitation is limited [*Swapna et al*., 2009]. Because $\rho_\theta{}'$ is different in the NPO and the SCS as a result of the SCSTF in the basin, and a consequence of the combined impacts from, e.g., strong mixing, or advection, in the LS, $\rho_\theta{}'$ indicates the water exchange between these two seas (Figure 2). Likewise, we infer the circulation and pathways of the SCS water from $\rho_\theta{}'$ at the standard depths of the WOA13. We use the three-layer definition of *Gan et al*. [2016b] to divide water column into three layers separated at 750 m and 1500 m, respectively. We further divide the lower layer defined in *Gan et al*. [2016b] into two layers separated at 2500 m, to better elaborate the migration of waters in the deep closed basin. Thus, the depths of the upper, intermediate, and lower layers, as well as the layer in the closed basin are defined as 0–750 m, 750–1500 m, 1500–2500 m, and 2500 m-bottom. In this paper, we refer to the combination of the lower layer and closed basin as the deep basin.

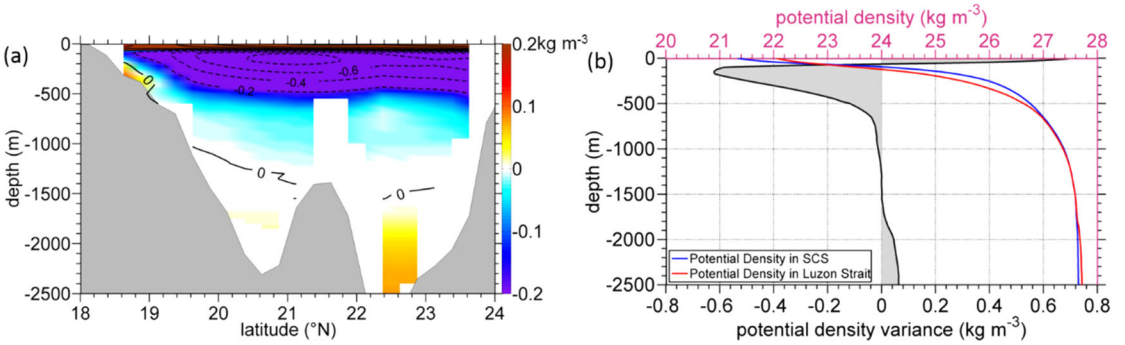

Figure 2. (a) The meridional $\rho_\theta{}'$ (kg m^{-3}) profile as function of depth and latitude along the section at 121.75°E in LS, and (b) profile of $\overline{\rho_\theta}$ (kg m^{-3}) averaged in LS (red) and in the SCS basin (blue). The shaded area in (b) denotes the meridionally averaged $\rho_\theta{}'$ (kg m^{-3}) in the SCS (blue) and over the section at 121.75°E (red), and for a better presentation, we ducted 1000 kg m^{-3} from the calculated potential density to get the $\overline{\rho_\theta}$ in Figure 2b.

2.1. ρ_θ' in LS

Figure 2a illustrates the ρ_θ' profile as a function of depth in the meridional section along 121.75°E (transect *M* in Figure 1a), where the deepest sill in LS is located. Figure 2b shows the vertical profile of ρ_θ' and $\overline{\rho_\theta}$ (meridionally averaged along transect *M*) in LS and $\overline{\rho_\theta}$ in the SCS basin. The $\overline{\rho_\theta}$ in the SCS (blue line in Figure 2b) is the reference we used to calculate the ρ_θ'.

A negative ρ_θ' in LS (Figure 2a) suggests that the intrusive water from the NPO is less dense than the SCS water in the upper layer (0–750 m), and thus the source of the higher $\rho_\theta(x,y,z)$ in the SCS is expected to be the upwelled waters from the depths. ρ_θ' in the intermediate layer (750–1500) in LS is also negative. Since flow in the intermediate layer in LS is outward, a negative ρ_θ' means that the intermediate water in the SCS is also denser than that in LS. This implies that there is an upwelling of denser waters from the lower layer of the SCS (Figure 2b) into the intermediate layer of the basin. In the lower layer of LS (Figure 2a), ρ_θ' is positive and increases northward, as also reported by *Qu et al*. [2006b]. This suggests an intrusion of denser NPO waters into the deep basin of the SCS and the intrusion occurs mainly in the northern part of LS. The water in the lower layer of the SCS is much less dense than the intrusive NPO water (Figure 2b), which is likely due to the subduction of intermediate water in the basin. Next, we analyze ρ_θ' in the SCS to find evidence and the location of the lower (intermediate) layer SCS water upwelling into the intermediate (upper) layer and the associated pathways of the water masses.

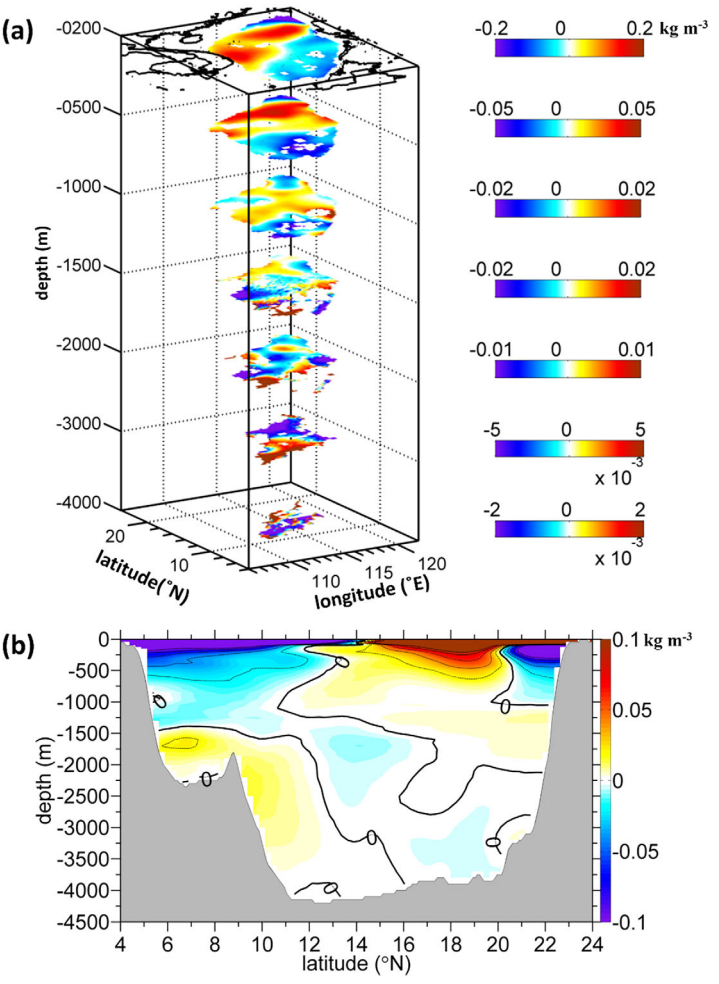

Figure 3. (a) Three-dimensional view of ρ_θ' at selected, but representative, layers of the SCS and (b) zonally averaged ρ_θ' (kg m^{-3}) as a function of depth and latitude in the SCS. ρ_θ' is retrieved from the annual means of the WOA13 data set.

2.2. Pathways of Water Masses Inferred From ρ_θ'

In order to better identify pathways of the SCS water, we show the horizontal distribution of ρ_θ' at representative layers of WOA13 in Figure 3a, and elucidate the zonally averaged ρ_θ' in the basin in Figure 3b.

In the three-dimension plane, upwelling of denser intermediate water is expected to occur in the northern and western SCS, immediately beneath the mixed layer (200 m and 500 m in Figure 3a), where we see a positive ρ_θ'. The subduction of lighter water in the upper layer into the intermediate layer may occur in the SSCS where ρ_θ' is negative at depths of 200 m and 500 m in Figure 3a.

We observe an extensive subduction of the upper layer water toward the intermediate layer at 1000 m, and a notable upwelling in the lower layer in the SSCS, as suggested by the respective negative and positive ρ_θ' in the regions. These vertical migrations of the water masses in the SSCS are also indicated by the respective negative and positive ρ_θ' in the intermediate layer and

in the lower layer (>1500 m) in Figure 3b. Similarly, extensive downwelling of intermediate water toward the lower layer likely occurs in the NSCS, where $\rho_\theta{}'$ is negative (Figure 3a).

The migration of the water masses inferred from $\rho_\theta{}'$ in LS (Figure 2) and that represented by $\rho_\theta{}'$ in the SCS basin (Figure 3) is consistent with each other. However, it requires validation from the three-dimensional SCS circulation. In fact, the linkage between these observation-based findings and the SCS circulation is consistent with that found in the numerical modeling study presented below.

3. Exchanging Flow and Circulation in the SCS

3.1. The Modeling System

We use the China Sea Multi-scale Ocean Modeling System (CMOMS) [*Gan et al*., 2016a] to further investigate the exchanging flow and general circulation in the SCS and to extrapolate the pathways that we presented in section 2. CMOMS is based on the Regional Ocean Modeling System (ROMS) [*Shchepetkin and McWilliams*, 2005], and the model domain covers the NPO and the entire China Seas (Bohai, Yellow Sea, East China Sea, and SCS) from approximately 0.95°N, 99°E in the southwest corner to the northeast corner of the Sea of Japan. The model has a horizontal resolution of about 0.1° and 30 levels over the stretched terrain following coordinates. The CMOMS nests with the global model of the Ocean General Circulation Model for the Earth Simulator (OFES) [*Masumoto et al*., 2004], and it includes both tidal and subtidal forcing along the open boundaries. We use a novel open boundary condition that jointly accommodates the tidal and subtidal forcing [*Liu and Gan*, 2016]. We initialize the model with the WOA13 hydrographic field, and it spins up for 50 years to quasi-steady state with climatological atmospheric and lateral fluxes. The model outputs are averaged over the last 5 year run, and the results are used in this study.

We have thoroughly validated the CMOMS by comparing simulated results with those obtained from various measurements and findings in previous studies. In particular, we have validated the extrinsic forcing of time-dependent, three-dimensional current system in the tropical NPO, transports through the straits around the periphery of the SCS, and corresponding intrinsic responses of circulation, hydrography, water masses and tides in the SCS. We have also validated the circulation of CMOMS by providing a consistent physics between the intrinsic responses of the circulation and extrinsic forcing of flow exchange with adjacent oceans. The dynamic configuration, numerical implementation, and validation of the CMOMS system are described in detail in *Gan et al*. [2016a,2016b]. The fact that the model is able to realistically capture the circulation and forcing conditions in the SCS establishes a level of confidence in the results to be presented in this study.

3.2. The General SCS Circulation

The pathway of the waters in the horizontal plane of the SCS is indicated by the vertically integrated transport function in the upper, intermediate, and lower layers, and in the closed basin (Figure 4). To illustrate the basin circulation better, we exclude the current over the continental shelves where the water is shallower than 200 m. CMOMS results explicitly show the existence of a three-layer circulation in the SCS basin (Figure 4, also see *Gan et al*., [2016b]). This three-layer circulation includes cyclonic circulation in the upper layer and in the deep basin. The intermediate circulation flows anti-cyclonically (Figure 4b).We analyze the basin circulation below.

3.2.1. Upper Layer

The transport stream function in five areas (areas A to E in Figure 4a) demonstrate the along-stream variation in the upper layer circulation. The figure clearly shows the extensive cyclonic circulation in the upper layer resulting from the KC intrusion and a positive wind stress curl [*Gan et al*., 2006; *Metzger*, 2003].

The volume transport of this cyclonic current is about 8 Sv over the western slope in the northwestern SCS of area A. The southwestward motion of the upper layer waters weakens toward the slope north of the Xisha Islands (Area B). This is also consistent with the AVISO observation (Figure 1b). In area B, a portion of the water (< 2 Sv) in the upper layer veers southeastward and crosses the central basin toward Mindoro Strait, before circulating cyclonically northward along the west coast of the Philippines. The major portion of the upper layer waters in area B flows further southward and the volume transport is intensified over the slope east of Vietnam (Area C) to form the WBC (~8 Sv). The invasive KC waters in the upper layer are mainly positioned over the slope to the shore-side of this cyclonic circulation, while the aforementioned

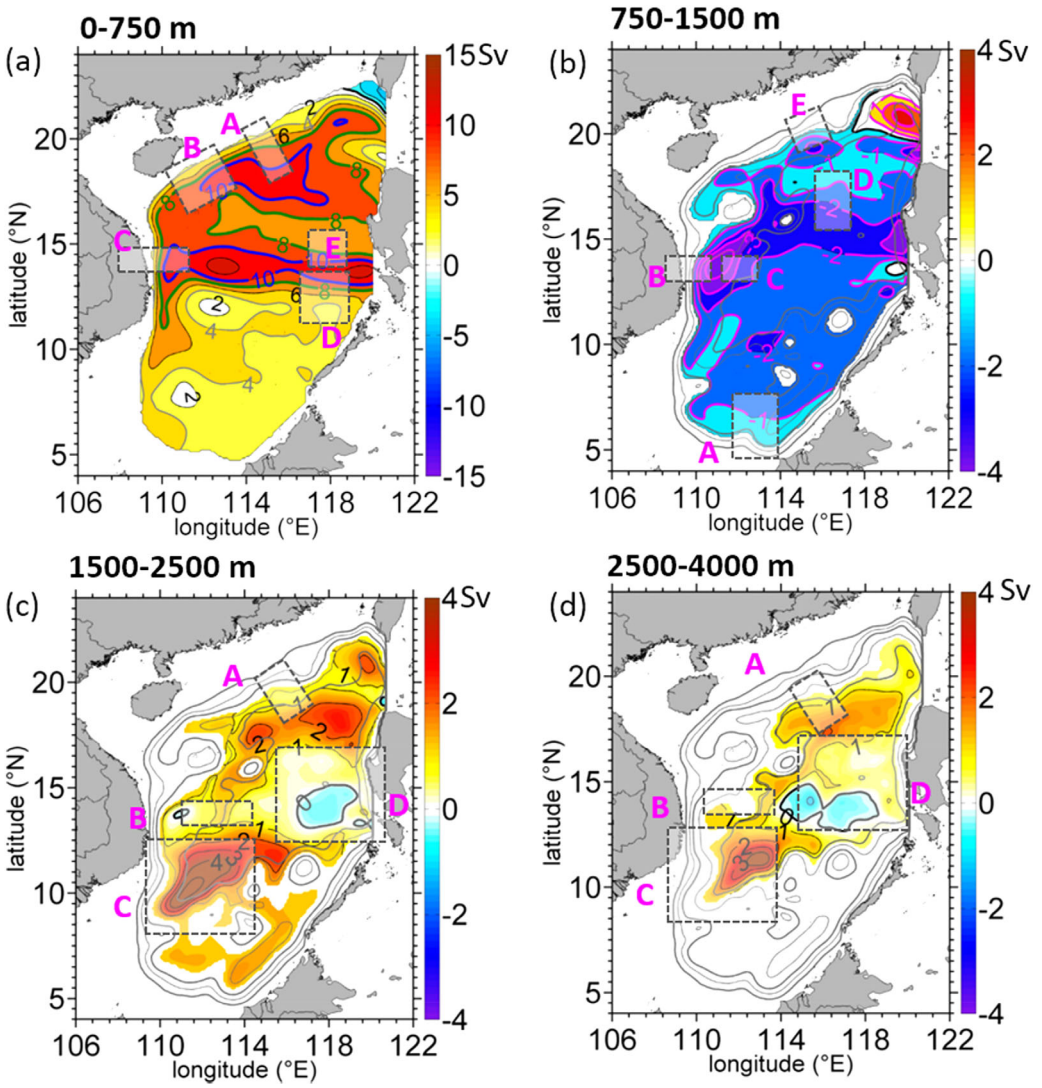

Figure 4. The transport stream function integrated in the (a) upper, (b) intermediate, (c) lower layers, and (d) closed basin of the SCS. The values over the continental shelf are excluded in Figure 4a. The color scale in Figure 4a is expanded for better presentation, and the model results are averaged for years 45–50 in CMOMS.

southeastward branch from area B is mainly confined over the slope to the sea-side. This notable difference in the spatial origin of these branching currents will be shown to play different roles in influencing the pathway of upper layer waters in the coming section 4.2.

The upper layer waters in area C evacuate further southward and decelerate in the SSCS. Its main stream veers northeastward toward Mindoro Strait (Area D). The volume transport in area D is about 6 Sv, and a portion (3∼4 Sv) of this transport recirculates without exiting the SCS through Mindoro Strait. Instead, the volume transport in area D flows back along the westward stream that is centered at 15°N in the central basin (Area E). The volume transport (2∼3 Sv) originating from area C in the SSCS is the major contributor to the eastward transport in Mindoro Strait (∼3 Sv in Figure 1b).

3.2.2. Intermediate Layer

The volume transport (∼1 Sv) of the anti-cyclonic circulation along the slope of the SSCS (Area A in Figure 4b) is much smaller than the volume transport in the upper layer. However, this anti-cyclonic motion of the intermediate waters is remarkably intensified over the slope east of Vietnam (area B in Figure 4b), and the northward excursion occurs beneath the main stream of the upper layer. In area B, the transport increases to about 4 Sv. The majority of the intermediate water, carried by this northward current (∼2 Sv), circulates along an intermediate anti-cyclonic cell over the slope at 13°N, southwest of the Xisha Islands (area C in

Figure 4b). A portion (∼1 Sv) of this northward current veers eastward and flows across the intermediate SCS basin (area D in Figure 4b) toward Mindoro Strait. The remaining portion (1∼2 Sv, in area E) evacuates northeastward and exits the SCS at the intermediate layer of LS.

The transport function in Figure 4b represents a westward invasion of intermediate NPO water into the northern part of LS. Although its magnitude is smaller than the eastward transport in the southern LS, the intermediate waters in NSCS and immediately west of LS are also extensively influenced by the NPO water.

3.2.3. Deep Basin

The deep circulation in the deep basin (>1500 m) can be divided into three sections composed of a weak cyclonic circulation in the NSCS, a strong cyclonic circulation in the SSCS, and an anti-cyclonic circulation in the eastern SCS to the west of Mindoro Strait (Figures 4c and 4d). The intrusive denser NPO water from the lower layer of LS (Figure 4c) induces a cyclonic circulation (∼2 Sv) in the basin immediately west of LS. It decelerates southwestward along the slope of the NSCS (1–2 Sv in area A, Figure 4c). A portion of this current (<1 Sv) flows southward along the slope east of Vietnam (area B in Figures 5c and 5d). Then, it is trapped by a notable and much stronger eddy-like cyclonic circulation (>5 Sv) in the SSCS (area C in Figures 5c and 5d). This cyclonic circulation centers at ∼11°N in the southernmost corner of the deep basin and is likely induced by the flow over a topographic trough. The cyclonic circulation of the NSCS and the SSCS are separated by an anti-cyclonic circulation in the deep basin west of Mindoro Strait (area D in Figures 4c and 4d).

3.3. The Exchanging Flow in LS

Figure 5 shows the profile of ρ_θ' (Figure 5a) and the eastward/outward (positive) and westward/inward (negative) volume flux (Figure 5b), meridionally integrated along the section at 121.75°E in LS (transect *M* in

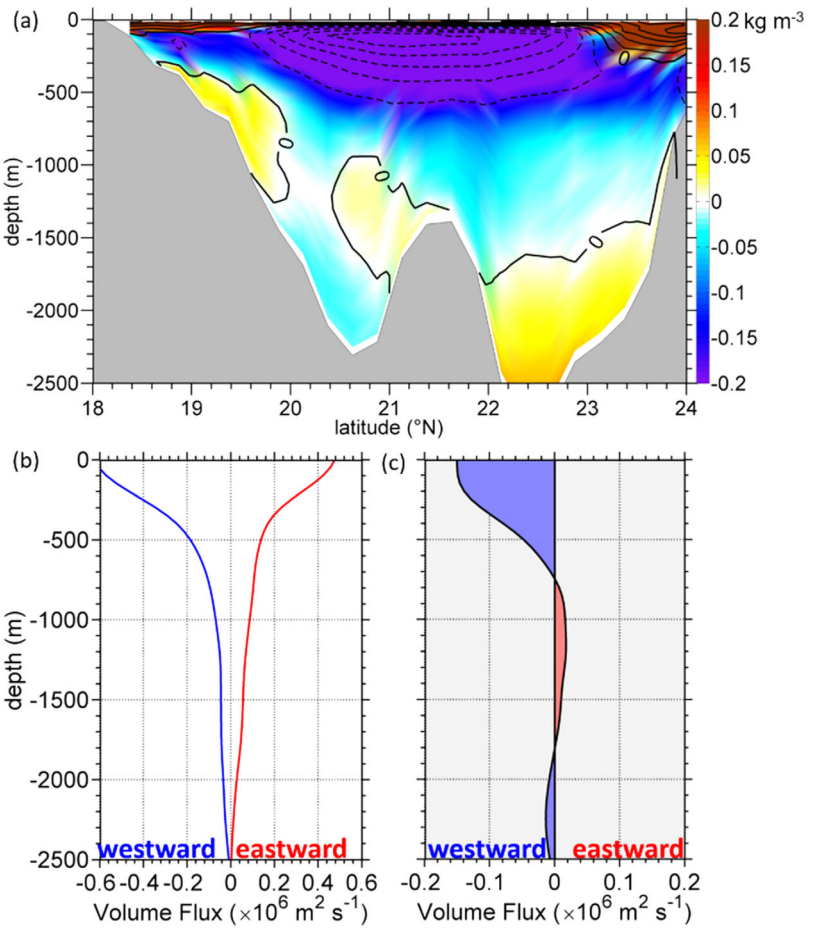

Figure 5. (a) The meridional ρ_θ' (kg m^{-3}) profile along the section at 121.75°E in LS, (b) profile of (blue) westward and (red) eastward volume flux, and (c) the net east-westward volume flux (shaded area) meridionally integrated in LS. ρ_θ' and volume flux are averaged for years 45–50 in CMOMS. The positive value in Figure 5b refers to an eastward transport.

Figure 1a). The net volume flux, which is a summation of the eastward and westward volume flux is illustrated in Figure 5c.

$\rho_\theta{}'$ in Figure 5a depicts agreement between the observed hydrographic nature of the three-layered exchanging flow (Figure 2a) and the CMOMS results in LS, e.g., the intrusion of much less dense KC water into the upper layer of the SCS. Consistent with the observations in Figure 2a, the simulated $\rho_\theta{}'$ profile from CMOMS shows eastward evacuation of the less dense SCS water in the intermediate layer, with positive and negative $\rho_\theta{}'$ at the southern and northern parts of LS, respectively. The larger and positive $\rho_\theta{}'$ in the deep ocean of the northern strait indicates that much denser NPO water has invaded in the lower layer of LS. The strength of the three-layered exchanging flow in LS is presented in Figures 5b and 5c. It is clear that the most extensive exchanging flow occurs in the upper layer. The net volume transport of the less dense intrusive KC water in the upper layer is approximately −5.9 Sv (Figure 5c), in which the inward and outward volume transports are approximately −22.3 Sv and 16.4 Sv (Figure 5b), respectively. Meanwhile, denser NPO water with a net volume transport of approximately −0.9 Sv intrudes into the SCS through the lower layer of LS (Figure 5c). The inward and outward volume transports in this layer are approximately −2.3 Sv and 1.4 Sv, respectively. The total transport exiting SCS through the other three straits around the SCS (Figure 1b) is approximately 5.4 Sv and it mainly occurs in the upper layer. This suggests an approximately 0.5 Sv subduction of water from the upper layer to the intermediate layer. The subducted water joins the upwelled water from the semiclosed lower layer of the SCS (∼−0.9 Sv) to form the net eastward transport of the SCS water into the intermediate layer of LS (∼1.4 Sv). Note that inward and outward volume transports still exist in the intermediate layer of LS. Although the net volume transport is small (∼1.4 Sv), the inward and outward volume transports are moderately large at approximately −6.1 Sv and ∼7.5 Sv, respectively. According to *Gan et al*. [2016b], this three-layered water exchange in the SCS is linked to the transports in the other straits surrounding the SCS (Figure 1b). This three-layered exchanging flow in LS also largely determines the pathways of the water in the SCS by altering the squeezing/stretching of waters in the basin through a lateral planetary vorticity flux.

4. Intrinsic Characteristics of Water Pathways in the SCS

The observed and simulated $\rho_\theta{}'$, and the flow field from CMOMS show that the extensive flow exchange in LS largely shapes the pathways of the water masses in the SCS. The three-layered SCS circulation (section 3) provides the general pathways of the SCS water masses. In this section, we further investigate the pathways of the SCS water masses by utilizing the parcel-tracking Euler technique [e.g., *Kuebel Cervantes et al*., 2003]. This approach defines the Lagrangian labels (X, Y), which are conserved variables advected by the three-dimensional circulation. This approach also avoids losing original identity of waters by mixing with ambient waters as that provided by nonconserved variables with diffusivity. The governing equations of the Lagrangian labels are expressed as

$$\frac{DX}{Dt}=0;\ \ \frac{DY}{Dt}=0, \tag{2}$$

in which $\frac{D}{Dt}=\frac{\partial}{\partial t}+u\frac{\partial}{\partial x}+v\frac{\partial}{\partial y}+w\frac{\partial}{\partial z}$, and (x, y, z) and (u, v, w) represent the spatial coordinates and the three-dimensional velocities, which are resultant from the complicated processes, e.g., mixing and advection, in the oceanic model, respectively. $\frac{\partial}{\partial t}$ denotes time differentiation. This technique transforms the Lagrangian trajectories to a continuous field of tracers. The distribution of the computed labels is highly consistent with a distribution that is solved using conventional Lagrangian trajectories [*Kuebel Cervantes and Allen*, 2006]. Simialr consistence is also found in our numerical experiments (see supporting information). Method with equation (2) represents the water parcel trajectories resolved by the velocities governed by the model dynamics with a parameterization of small-scale turbulence. The effect due to interaction between advection and diffusion [e.g., *Taylor*, 1953, 1954] may not be well represented in the model. However, we believe that our analysis based on the model velocities provide useful information for such interaction and for Largrangian information in the SCS.

We initialize the labels (X, Y) by the longitude and latitude of the CMOMS grids in the entire computational domain. This labeling allows equation (2) to preserve the original spatial identity of the water. We solve equation (2) using the standard kernel for passive tracers in ROMS by excluding the horizontal and vertical diffusions. We apply a multidimensional positive-definite advection algorithm [*Smolarkiewicz*, 1984] to

handle the advection of the labels in equation (2) in order to minimize numerical diffusion. The boundary values for these labels are prescribed to the initial condition. The tracers experiment is started from year 21 of the CMOMS run, when a quasi-steady state has been achieved [*Gan et al.*, 2016a]. We run this tracers experiment for an additional 50 years to allow the water that was initially inside the SCS (SCS water) to be sufficiently refreshed by intrusive NPO water (non-SCS water). The total run of the tracers simulation is 70 years, with the tracers are injected at the beginning of the year 21. The area of the defined SCS water is illustrated in Figure 1a. Incorporating equation (2) into CMOMS allows us to distinguish the origin of the Lagrangian labels (X, Y). Then, by following the time step of the simulation at each location of the SCS (grid point in CMOMS). We record the time when the non-SCS water appears, and establish *ReT* at each particular location. In this way, we compose a three-dimensional *ReT* in the SCS. During this process, isolines of *ReT* sketch the pathways of the non-SCS water that is progressively spreading in the basin. This definition is different from the traditional flushing time, which is obtained by divided the volume of the concerned waters with exchanging flow rate along lateral boundary. By using this definition, we can better reveal the nature of the three-dimensional variation of *ReT* in the SCS basin.

4.1. *ReT* of SCS Water Masses

Figure 6 illustrates the time series of the percentage of SCS water being replaced by the invasive non-SCS water as a function of the water depth. The 100% contour (bold black line in Figure 6) represents the time when the basin is completely occupied by non-SCS waters at certain depths and is called the maximum *ReT* (ReT_{max}), which has never been reported in previous studies. So, the relationship between the *ReT* and ReT_{max} can be expressed as

$$ReT_{max}\ (z) = \max\left[ReT(x, y, z)\right]. \tag{3}$$

Our result shows that ReT_{max} in the entire SCS is generally shorter than 45 years. Figure 6 clearly illustrates that ReT_{max} increases with depth. The water in the near-surface layer ($<$ 200 m) is refreshed in about 3 years. This water is replaced by the KC water cyclonically spreading through the upper layer of LS (Figures 4b and 5). ReT_{max} in the upper layer, where the pycnocline is located (Figure 2b), rapidly increases to approximately 32 years at 750 m. ReT_{max} keeps increasing to its maxima in the intermediate layer ($\sim$42 years) and the upper part of the lower ($\sim$44 years) layer. It slightly reduces to approximately 40 years in the closed basin, where the water is much less stratified (Figure 2b). It will be explicitly expressed in the later contents of this section (Figure 7c) that there is a narrow but deep trough ($\sim$ 2430 m) between 114–117°E and 6–8°N in the southernmost of intermediate SSCS waters that have limited communication with the rest of the waters, and cause a sharp increment of ReT_{max} at $\sim$2200 m. In order to better reveal the variation of ReT_{max}, we analyze the amount of time needed to replace 90% of the SCS water masses in the water column. It further confirms that the longest ReT_{max} as a function of depth mainly occurs in the intermediate layer, since it takes approximately 38 years for 90% of the intermediate water to be refreshed, whereas the time needed for the

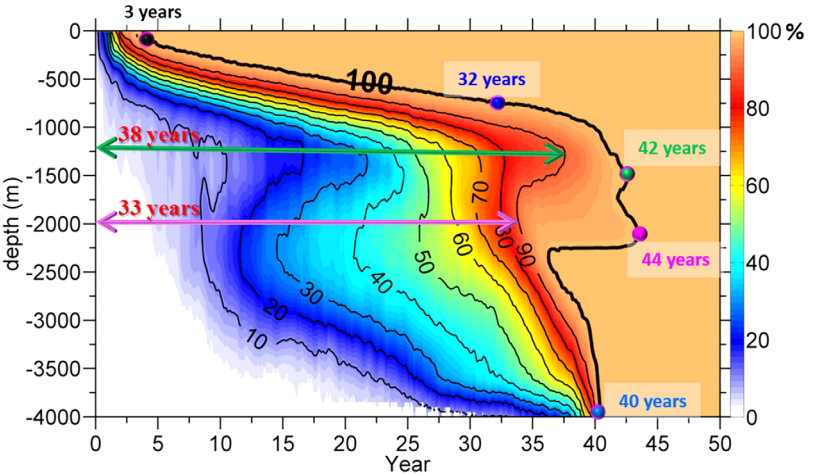

Figure 6. Time series of the percentage of water that is refreshed in the SCS as a function of depth.

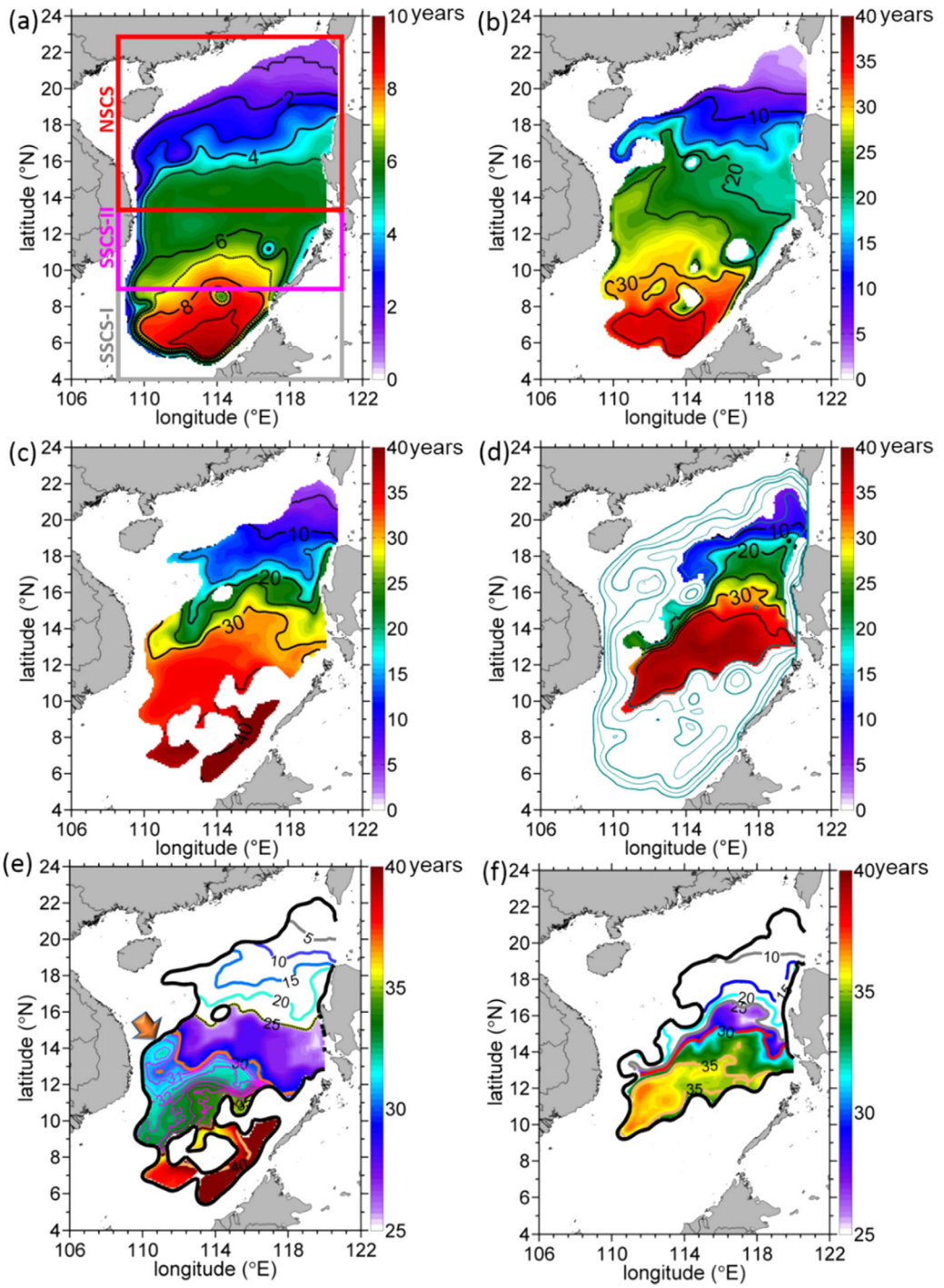

Figure 7. *ReT* averaged in the (a) upper, (b) intermediate, (c) lower layers, and (d) closed basin of the SCS. The *ReT* distribution at 1500 m and 2500 m of the SCS is illustrated in Figure 7e and Figure 7f, respectively. The values over the continental shelf are excluded in Figure 7a, and the color scale in Figure 7a is reduced for better presentation of the *ReT* variation in the upper layer. The color scale is also reduced in Figure 7e and Figure 7f to better reveal the characteristics of *ReT* in the SSCS.

same to happen in the lower layer is much shorter (~33 years). Unlike what previous studies have proposed [e.g., *Yang et al.*, 2012], that ReT_{max} increases monotonically with depth, this longest ReT_{max} in the intermediate layer suggests that the formation of intermediate water is deferred, under the prevailing anti-cyclonic circulation (Figure 4b).

4.2. Linking the Layered Waters

In the previous section, we have investigated the characteristics of ReT_{max}, which varies solely in the vertical direction. The spatial variation in *ReT* for waters at individual locations of the SCS will be analyzed in this section. The vertically averaged *ReT* in the upper, intermediate, and lower layers, and in the closed basin is illustrated in Figures 7a–7d. We present the horizontal maps of *ReT* at 1500 m (between the intermediate and lower layers) and 2500 m (between the lower layer and the closed basin) in Figures 7e and 7f to better reveal the pathways of the waters at the interfaces of these layers. Figure 8a illustrates the zonally averaged *ReT* profile in the basin. To more clearly present the three-dimensional variation in *ReT* in the SCS, we partition the basin into three areas in the meridional direction (Figure 7a). These areas represent the shallow basin at the southernmost point of the SSCS (SSCS-I), the rest of the SSCS basin (SSCS-II) with a deeper and steeper slope, and the NSCS. The meridionally averaged *ReT* profiles over these three regions are illustrated in Figures 8b–8d, and the meridional variation of *ReT* from the southernmost (SSCS-I) to the northernmost (NSCS) of the basin is thereafter presented in Figure 8a.

We find that *ReT* of the SCS water generally increases southward in the entire water column, and a *ReT* minima (ReT_{min}) exists in the NSCS immediately west of LS (Figures 7 and 8a). This ReT_{min} increases from less than 1 year in the upper layer to approximately 10 years in the deep basin (Figures 8a and 8d). The SCS water that is geographically closer to the source region of the non-SCS water is refreshed in a shorter period of time by the exchanging flow through LS (Figure 5b). This finding is intuitive, but has largely been ignored in traditional studies.

In the remainder of this section, we will investigate the pathways of SCS waters by analyzing *ReT* in different layers.

4.2.1. Upper Layer

The isolines of a relatively short *ReT* (<2 years) extend westward and southward across the NSCS basin in the upper layer (Figure 7a), where a cyclonic circulation prevails (Figure 4a). The main stream of this current becomes thinner toward the lower latitude (Figure 8a). The majority of the cyclonically propagating water moves further southward along the slope east of Vietnam and enters the SSCS. This water then veers northeastward along the southeast side of the slope in the SSCS (SSCS-I region in Figure 7a), and exits the basin through Mindoro Strait (SSCS-II). The shorter *ReT* (<4 years) along the west coast of the Palawan Archipelago reveals extensive exchanges between the SCS and the Sulu Sea, which is also identified in *Gan et al.* [2016a] by an eastward excursion of the SCS water above 500 m. The *ReT* isolines (Figure 8a) in the upper

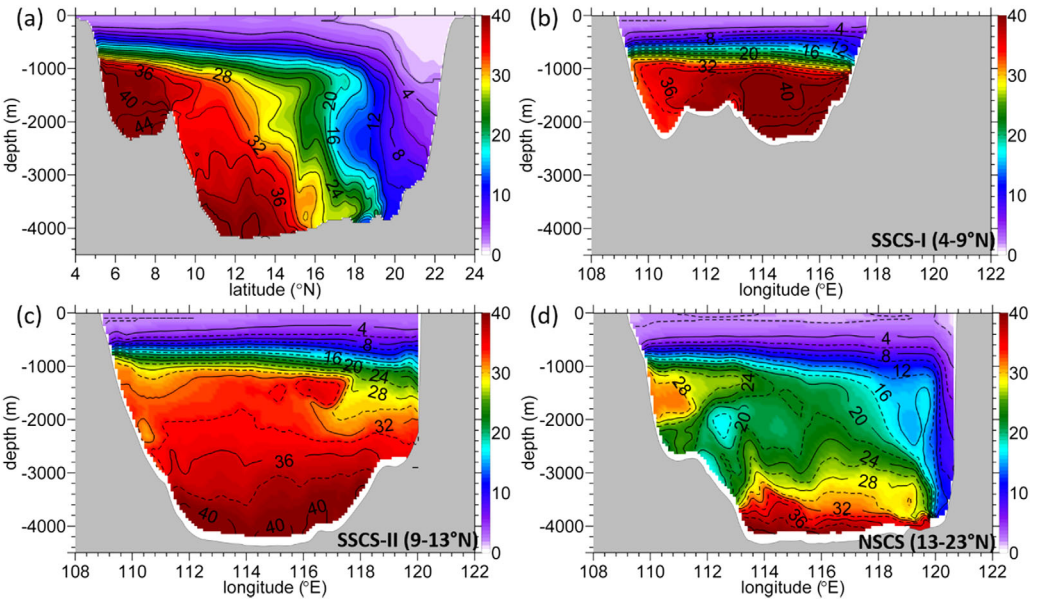

Figure 8. (a) Zonally averaged *ReT* in the SCS, and the meridionally average *ReT* in the areas indicated by (b) SSCS-I, (c) SSCS-II, and (d) NSCS, whose location is illustrated in Figure 7a.

layer suggest that horizontal transport due to the cyclonic circulation along the slope mainly guides the motion of the SCS water from the north toward the south.

Figure 7a shows a large seaward gradient of *ReT* over the slope to northeast of the Xisha Islands, in which a smaller *ReT* (<2 years) and a larger (3–5 years) *ReT* are positioned to the shore-side or sea-side of the southwestward slope current. This finding suggests that the invasive KC waters from LS cannot directly branch southeastward across the basin toward Mindoro Strait from the Xisha Islands (area B in Figure 4a). Instead, the waters in the upper layer, flowing northeastward along approximately 10°N, form the majority of the waters exiting Mindoro Strait. This finding is consistent with what is reflected by the upper layer transport stream function (Figure 4a).

4.2.2. Intermediate Layer

It is clear that the impact of the non-SCS water in refreshing the intermediate water is limited in the NSCS, and the intermediate water is flushed within ~25 years (Figure 7b). The isolines of the *ReT* (e.g., 25 years in Figure 7b) sketch a northward stream over the slope east of Vietnam, in response to an extensive northward current (Figure 4b). In the intermediate layer, *ReT* is the longest (Figure 8d) over the slope east of Vietnam (Figures 7b and 8d). The formation of intermediate water is thereby deferred, as we can also see in Figure 6. We observe upwelling of lower layer water which has a longer *ReT* in the SSCS-I region, as shown in the southernmost of Figure 8a, and over the slope between 113°E and 115°E (Figure 8b). The subducted upper layer water is represented by the isolines with a shorter *ReT* along the western SSCS-I slope between 110°E and 112°E (Figure 8b). The intermediate layer is, consequently, formed by the subducted upper layer water and the upwelled lower layer water in the SSCS, and this finding is consistent with that from $\rho_\theta{}'$ in section 2.2. Thereby, when the NSCS are refreshed by invasive NPO waters from the lower layer of LS, the deep waters of SSCS will be upwelled to the intermediate layer, and carried northward by the anti-cyclonic circulation in this layer. This portion of SCS waters is thereafter "shielded" from being updated by those invasive NPO waters. This finding explains the longest ReT_{max} in the intermediate layer (Figure 6).

4.2.3. Deep Basin

The closed basin of the SCS, immediately west of LS, is completely flushed by intrusive non-SCS water from the lower layer of LS in 10 to 12 years. The fact that this is similar to the *ReT* in the deep basin (Figure 8d) suggests that the intrusive water from LS cascades downward into the closed basin after entering the SCS. In addition, there is a weaker southward branch of the intrusive non-SCS water along the west coast of the Philippines. The isolines with a relatively short *ReT* (e.g., 15~25 years in Figure 7c) extend westward and southward along the main stream of the deep cyclonic circulation (Figures 4c and 4d). However, it is clear that these isolines do not extend over the slope east of Vietnam, where an extensive northward gradient of *ReT* positions. This indicates a slowing formation of the deep water in the SSCS. The water in the deep basin of the NSCS is formed within ~25 years. It has a *ReT* of less than 25 years and it occupies approximately 37.8% of the total volume of the deep basin.

An extensive subduction of the intermediate water over the slope east of Vietnam prevents southward evacuation of the intrusive non-SCS water along the slope in the northwestern SCS in this layer. This subduction is revealed by the water masses with a longer *ReT* (>30.5 years) at 1500 m east of Vietnam and between 13°N and 14°N (arrow in Figure 7e), and the observed negative $\rho_\theta{}'$ in Figure 3. The deep SSCS water formed from the intrusive water in the lower layer of LS is not able to reach this region, and the *ReT* (> 30 years) is horizontally homogeneous (Figures 7c and 7d) due to the existence of a strong eddy-like cyclonic circulation (Figures 5c and 5d). A longer *ReT* over the western slope at 2500 m in the SSCS (Figure 7f) indicates the path traversed by the upwelled water from the closed deep basin to the lower layer, while a shorter *ReT* at the eastern slope reveals the path traversed by the subducted lower layer water to locally refresh the SSCS water in the closed basin.

5. Fate of Deep Intrusive Water

Up to this point, we have presented the observed and simulated pathways of the SCS water masses that arise from the exchanging flow through LS and from the interchange in the layered waters. In this section, we investigate the fate of the intrusive denser water from the lower layer of LS. This water is hypothesized to move downward in the NSCS and induce upwelling in the far basin to compensate for the injection of the intrusive denser NPO water in LS [e.g., *Fang et al.*, 2009]. However, this hypothesis cannot distinguish

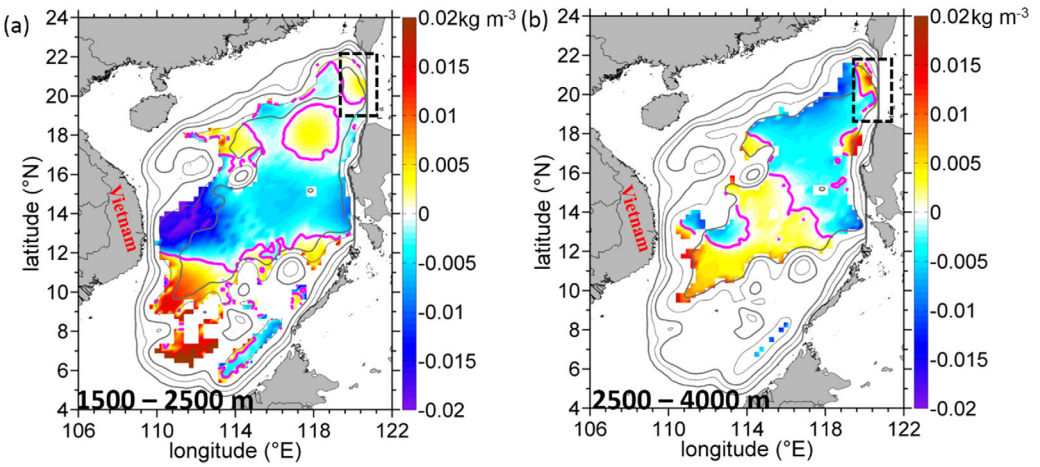

Figure 9. Horizontal distribution of ρ_θ' in the (a) lower layer (1500–2500 m) and (b) the closed basin (>2500 m) in the SCS and from the WOA13 data set.

the three-dimensional varied pathways and *ReT* of SCS waters, as well as the fate of these intrusive deep waters in the basin. To investigate the fate of the deep intrusive NPO water after it enters the SCS from the lower layer of LS, we use vertically averaged ρ_θ' from WOA13 observations in the lower layer between 1500 and 2500 m and in the closed basin with a water depth exceeding 2500 m (Figure 9).

The positive ρ_θ', in the lower layer of the NSCS immediately west of LS (dashed black box in Figure 9a), shows an intrusion of the denser NPO water, which locally cascades into the closed basin (Figure 9b). The intrusive water flows southwestward along the slope in the northwestern SCS (Figure 9a). However, it has little influence on the deeper layer in the NSCS, where ρ_θ' is largely negative (Figure 9b). This negative ρ_θ' in the NSCS is consistent with the discussion in section 2.2 and suggests that the water in the closed basin should be diluted by the water subducted from the intermediate layer to preserve its lower density.

To better illustrate the pathway of the deep SCS water, we show the vertically-averaged (1500–3000 m) *ReT*, along- and cross-slope velocity, and the vertical velocity along the 3000 m isobath (Figure 10a) that encircles the deep basin (Figures 10b–10e). The along-slope variability of *ReT* and velocities are highly consistent with the previous discussion, for example, the extensive eddy-like cyclonic circulation southwest of the deep basin (Figure 10c). The cross-slope (Figure 10d) and the vertical velocities (Figure 10e) vary coherently with a correlation coefficient of approximately 0.73, with 95% confidence interval. The correlation coefficient between the vertical and along-shore velocities is approximately 0.42. These correlation coefficients suggest that the migration of deep water is mainly induced by the cyclonic circulation in response to the slope topography in the deep SCS, instead of by the bottom friction which would make the latter correlation coefficient larger.

The pathway of the deep water in the SSCS is critically governed by the locally intensified eddy-like cyclonic circulation southwest of the deep basin (Figure 10c and area D in Figure 4d). Along the western side of this cyclonic circulation, the upslope invasion of deep water is at a maximum, where the shoreward and vertical velocities are approximately -9.6×10^{-3} m s^{-1} and 3.2×10^{-5} m s^{-1}, respectively (Figures 10d and 10e). On the southernmost slope of the SSCS, and along the eastern side of this cyclonic circulation, the water shifts to a downslope pathway (Figure 10f), and the maximum cross-slope and vertical velocities are approximately 9.5×10^{-3} m s^{-1} and -5.8×10^{-5} m s^{-1}, respectively. Then, the cross-slope migration of the deep SCS waters weakens along the main stream of the cyclonic circulation toward Mindoro Strait. We can now conclude that the formation of water in the SSCS, with *ReT* generally exceeding 30 years, is determined by a three-dimensional circulation, in which the upslope (downslope) transport of the deep water occurs along the western (eastern) side of the eddy-like cyclonic circulation to refresh the deep water in approximately 40 years. This process is also presented in Figure 8c, in which the isolines of *ReT* = 32 years rise on the western slope and cascade on the eastern slope of the SSCS-II region.

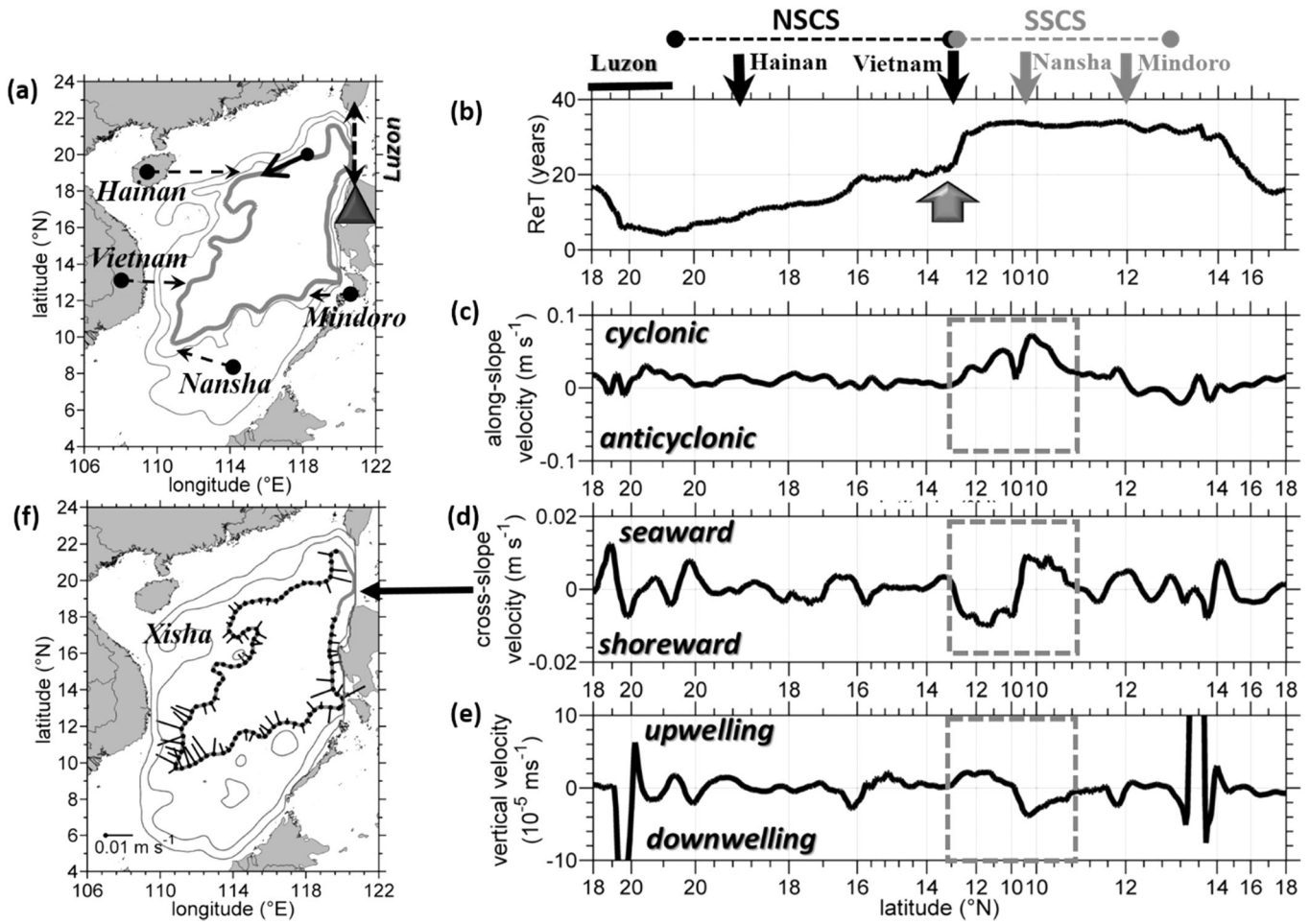

Figure 10. (a) The 3000 m isobath encircling the SCS deep basin, and along-isobath variations in (b) *ReT*, (c) along-slope velocity, (d) cross-slope velocity, and (e) vertical velocity averaged in the deep SCS basin. The along-slope variation in the cross-slope velocity along the 3000 m isobath is illustrated in Figure 10f. Positive values depict cyclonic circulation in Figure 10c, seaward velocity in Figure 10d, and upward velocity in Figure 10e. The starting point shown in (b-e) is marked by the black triangle in Figure 10a.

6. Summary

We use the climatological WOA13 hydrographic data and the numerical solutions from CMOMS to investigate the pathways of water masses in the SCS. Extensive evidence shows that the NPO and the SCS waters are connected via LS, and that the water pathway in the basin varies spatially. This research presents the first three-dimensional picture of the spatially varying *ReT* of waters in the SCS, based on circulation and dynamics framework of *Gan et al*. [2006, 2016a, 2016b]. The study of pathway of waters and *ReT* dynamically links the intrinsic three-dimensional circulation in the SCS with extrinsic forcing from the NPO. The findings about the pathways of the migrating water in the SCS are summarized in Figure 11.

An extensive westward intrusion of the KC (∼5.9 Sv) is identified in the upper layer of LS, where a stream of less dense NPO water flows into the upper layer of the SCS. This intrusive current weakens southwestward while flowing cyclonically along the slope in the northwestern SCS. It subsequently veers southward and accelerates to approximately 8 Sv over the slope east of Vietnam in the SSCS. This cyclonic circulation connects the SCS to the neighboring oceans through Karimata and Mindoro Straits.

The CMOMS simulation presents an extensive eastward transport of denser SCS water in the intermediate layer of LS (∼1.4 Sv). This outflow originates from an anti-cyclonic circulation in the intermediate layer of the SCS. We identify the origin of this outflow to be the SSCS. The denser SCS intermediate water intensifies over the slope east of Vietnam to approximately 4 Sv. A moderate portion (1∼2 Sv) of this intensified current flows further north along the slope in the northwestern SCS before exiting through the intermediate layer of LS.

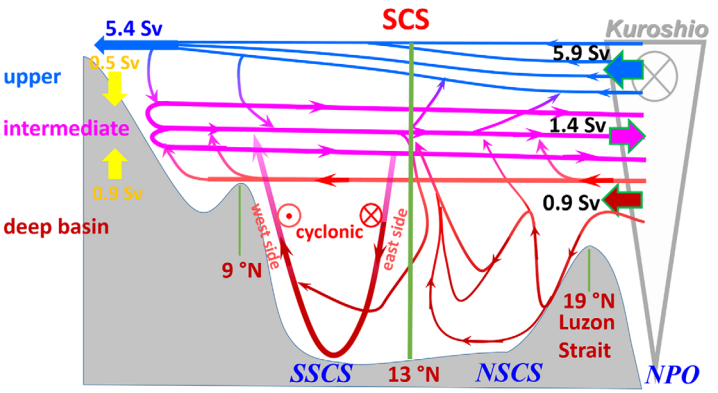

Figure 11. Schematic summarizing the transport and pathways of water in the SCS.

We observe an invasion of denser NPO waters in the lower layer of LS (~0.9 Sv). This intrusive lower layer current imposes a cyclonic circulation (1–2 Sv) in the deep basin (> 1500 m) of the northwestern SCS. Its main stream then veers southward over the slope east of Vietnam. The water then intrudes into an area near the southernmost slope of the SSCS where an extensively intensified and eddy-like cyclonic circulation (> 5 Sv) is located.

The observed ρ_θ' from the WOA13 validates the simulated exchanging flow and the cyclonic-anticyclonic-cyclonic three-layer circulation in the SCS. This circulation structure coherently guides the pathway of the SCS water, which is critical for sustaining the basin-scale SCS circulation. We find a strong ventilation of denser intermediate water in the NSCS and over the slope east of Vietnam, where it upwells into the upper layer. The upper layer water sink into the intermediate layer in the SSCS. The subducted upper layer water converges with the extensively upwelled denser water from the deep basin to form the intermediate water in the SSCS. The intermediate water flows northward and northeastward along the slope in the western SCS following the basin-scale anti-cyclonic circulation. The westward intruding denser NPO water in the lower layer of LS sinks into the closed basin immediately west of LS and bifurcates southwestward along the slope in the NSCS and southward along the west coast of the Philippines. The subducted intermediate water mainly occupies the central deep basin in the NSCS.

We use Eulerian analyses to track the water movement and identify the pathways of intrusive NPO water through LS. We find that the *ReT* of the SCS water is generally shorter than 45 years, and its magnitude increases deeper into the basin and closer to the south. This pattern shows that the SCS water, which is geographically closer to the source region of non-SCS water in LS, will be completely refreshed in a shorter period of time.

The water in the upper layer of the SCS is quickly refreshed within 3 years by the horizontal spreading of the intrusive NPO water through the upper layer of LS. The upper layer in the SSCS has a longer *ReT* (~10 years) where subduction of water occurs. The *ReT* of the SSCS water increases to its maximum (~42 years) in the intermediate layer and then reduces to approximately 40 years in the deep basin. The *ReT* distribution field further confirms that the intermediate water forms in the SSCS and then flows following the anticyclonic circulation. This process defers the formation of intermediate water and results in the maximum *ReT* in this layer. The impact of the intrusive deep NPO water from LS is limited in the NSCS, where the affected waters with *ReT* <25 years occupy approximately 37.8% of the total volume of the deep basin. The southwestward movement of this intrusive water ceases at approximately 13°N along the slope east of Vietnam, where the intermediate water travels extensively downward. The water in the deep basin of the SSCS has a much longer *ReT* than the water in the NSCS. Our results suggest that the deep water formation in the SSCS is mainly regulated by a pathway of three-dimensional circulation, which is induced by an eddy-like cyclonic circulation over a topographic trough at the southernmost tip of the basin. We find that subduction of the intermediate water along the eastern side of this cyclonic circulation is the source of the deep water, and the deep water mainly upwells into the intermediate layer along the western side of the cyclonic circulation.

Acknowledgments
This research was supported by the National Key Basic Research Development Program (2014CB441501; 2015CB954004), and the Hong Kong Research Grants Council (GRF16204915 and GRF 16206516). We are also grateful to the support of The National Supercomputing Center of Tianjin. The Archiving, Validation, and Interpretation of Satellite Oceanographic (AVISO) data were obtained freely from https://www.aviso.altimetry.fr/en/my-aviso.html. WOA13 data were obtained from https://www.nodc.noaa.gov/OC5/woa13/. All of the numerical information is provided in the figures produced by solving equations in the Regional Ocean Modeling System (ROMS) The source code of ROMS can be downloaded at https://www.myroms.org/.

References

Broecker, W. S., W. C. Patzert, J. R. Toggweiler, and M. Stuiver (1986), Hydrography, chemistry, and radioisotopes in the Southeast-Asian Basins, *J. Geophys. Res.*, *91*, 14,345–14,354, doi:10.1029/Jc091ic12p14345.

Chao, S. Y., P. T. Shaw, and S. Y. Wu (1996), Deep water ventilation in the South China Sea, *Deep Sea Res., Part I*, *43*(4), 445–466, doi:10.1016/0967-0637(96)00025-8.

Chou, W. C., D. D. Sheu, C. T. A. Chen, L. S. Wen, Y. Yang, and C. L. Wei (2007), Transport of the South China Sea subsurface water outflow and its influence on carbon chemistry of Kuroshio waters off southeastern Taiwan, *J. Geophys Res.*, *112*, C12008, doi:10.1029/2007JC004087.

Fang, G. H., Y. G. Wang, Z. X. Wei, Y. Fang, F. L. Qiao, and X. M. Hu (2009), Interocean circulation and heat and freshwater budgets of the South China Sea based on a numerical model, *Dyn. Atmos. Oceans*, *47*(1–3), 55–72, doi:10.1016/j.dynatmoce.2008.09.003.

Gačić, M., G. Civitarese, G. Eusebi Borzelli, V. Kovačević, P. M. Poulain, A. Theocharis, M. Menna, A. Catucci, and N. Zarokanellos (2011), On the relationship between the decadal oscillations of the northern Ionian Sea and the salinity distributions in the eastern Mediterranean, *J. Geophys. Res.*, *116*, C12002, doi:10.1029/2011JC007280.

Gan, J. P., H. Li, E. N. Curchitser, and D. B. Haidvogel (2006), Modeling South China sea circulation: Response to seasonal forcing regimes, *J. Geophys. Res.*, *111*, C06034, doi:10.1029/2005JC003298.

Gan, J. P., Z. Q. Liu, and L. L. Liang (2016a), Numerical modeling of intrinsically and extrinsically forced seasonal circulation in the China Seas: A kinematic study, *J. Geophys. Res. Oceans*, *121*, 4697–4715, doi:10.1002/2016JC011800.

Gan, J. P., Z. Q. Liu, and C. R. Hui (2016b), A three-layer alternating spinning circulation in the South China Sea, *J. Phys. Oceanogr.*, *46*, 2309–2315, doi:10.1175/JPO-D-16-0044.

Gascard, J. C. (1978), Mediterranean Deep-water formation baroclinic instability and oceanic eddies, *Oceanol. Acta*, *1*(3), 315–330.

Kuebel Cervantes, B., and J. S. Allen (2006), Numerical model simulations of continental shelf flows off northern California, *Deep Sea Res., Part II*, *53*(25), 2956–2984.

Kuebel Cervantes, B., J. S. Allen, and R. Samelson (2003), A modeling study of Eulerian and Lagrangian aspects of shelf circulation off Duck, North Carolina, *J. Phys. Oceanogr.*, *33*(10), 2070–2092.

Lan, J., N. N. Zhang, and Y. Wang (2013), On the dynamics of the South China Sea deep circulation, *J. Geophys. Res. Oceans*, *118*, 1206–1210, doi:10.1002/jgrc.20104.

Lascaratos, A., W. Roether, K. Nittis, and B. Klein (1999), Recent changes in deep water formation and spreading in the eastern Mediterranean Sea: A review, *Prog. Oceanogr.*, *44*(1–3), 5–36, doi:10.1016/S0079-6611(99)00019-1.

Li, L., and T. D. Qu (2006), Thermohaline circulation in the deep South China Sea basin inferred from oxygen distributions, *J. Geophys. Res.*, *111*, C05017, doi:10.1029/2005JC003164.

Liu, Z. Q., and J. P. Gan (2016), Open boundary conditions for tidally and subtidally forced circulation in a limited-area coastal model using the Regional Ocean Modeling System (ROMS), *J. Geophys. Res. Oceans*, *121*, 6184–6203, doi:10.1002/2016JC011975.

Metzger, E. J. (2003), Upper ocean sensitivity to wind forcing in the South China Sea, *J. Oceanogr.*, *59*(6), 783–798, doi:10.1023/B:JOCE.0000009570.41358.C5.

Qu, T., H. Mitsudera, and T. Yamagata (2000), Intrusion of the North Pacific waters into the South China Sea, *J. Geophys. Res.*, *105*, 6415–6424, doi:10.1029/1999JC900323.

Qu, T., Y. Du, and H. Sasaki (2006a), South China Sea throughflow: A heat and freshwater conveyor, *Geophys. Res. Lett.*, *33*, L23617, doi:10.1029/2006GL028350.

Qu, T., J. B. Girton, and J. A. Whitehead (2006b), Deepwater overflow through Luzon Strait, *J. Geophys. Res.*, *111*, C01002, doi:10.1029/2005JC003139.

Qu, T., Y. T. Song, and T. Yamagata (2009), An introduction to the South China Sea throughflow: Its dynamics, variability, and application for climate, *Dyn. Atmos. Oceans*, *47*(1–3), 3–14, doi:10.1016/j.dynatmoce.2008.05.001.

Masumoto, Y., et al. (2004), A fifty-year eddy-resolving simulation of the world ocean–Preliminary outcomes of OFES (OGCM for the Earth Simulator), *J. Earth Simulator*, *1*, 35–56.

Shchepetkin, A. F., and J. C. McWilliams (2005), The regional oceanic modeling system (ROMS): A split-explicit, free-surface, topography-following-coordinate oceanic model, *Ocean Modell.*, *9*(4), 347–404, doi:10.1016/j.ocemod.2004.08.002.

Shu, Y., H. Xue, D. Wang, F. Chai, Q. Xie, J. Yao, and J. Xiao (2014), Meridional overturning circulation in the South China Sea envisioned from the high-resolution global reanalysis data GLBa0. 08, *J. Geophys. Res. Oceans*, *119*, 3012–3028, doi:10.1002/2013JC009583.

Smolarkiewicz, P. K. (1984), A fully multidimensional positive definite advection transport algorithm with small implicit diffusion, *J. Comput. Phys.*, *54*(2), 325–362, doi:10.1016/0021-9991(84)90121-9.

Sofianos, S., and W. E. Johns (2015), Water mass formation, overturning circulation, and the exchange of the Red Sea with the adjacent basins, in *The Red Sea*, edited by N. M. A. Rasul and I. C. F. Stewar, pp. 343–353, Springer, Berlin.

Swapna, P., J. P. Gan, A. Lau, and J. Fung (2009), On the warm/cold regime shift in the South China Sea: Observation and modeling study, *Deep Sea Res., Part I*, *56*(7), 1039–1056, doi:10.1016/j.dsr.2009.03.008.

Taylor, G. I. (1953), Dispersion of solute matter in solvent flowing slowly through a tube, *Proc. R. Soc. London, Ser. A*, *219*, 186–203.

Taylor, G. I. (1954), The dispersion of matter in turbulent flow through a pipe, *Proc. R. Soc. London, Ser. A*, *223*, 446–468.

Wu, C. R., and Y. C. Hsin (2012), The forcing mechanism leading to the Kuroshio intrusion into the South China Sea, *J. Geophys. Res.*, *117*, C07015, doi:10.1029/2012JC007968.

Xu, F. H., and L. Y. Oey (2014), State analysis using the Local Ensemble Transform Kalman Filter (LETKF) and the three-layer circulation structure of the Luzon Strait and the South China Sea, *Ocean Dyn.*, *64*(6), 905–923, doi:10.1007/s10236-014-0720-y.

Yang, S. C., D. C. Lee, and T. Y. Ho (2012), The isotopic composition of Cadmium in the water column of the South China Sea, *Geochim. Cosmochim. Acta*, *98*, 66–77, doi:10.1016/j.gca.2012.09.022.

Zhou, C., W. Zhao, J. W. Tian, Q. X. Yang, and T. D. Qu (2014), Variability of the deep-water overflow in the Luzon Strait, *J. Phys. Oceanogr.*, *44*(11), 2972–2986, doi:10.1175/Jpo-D-14-0113.1.

Zweng, M., J. Reagan, J. Antonov, R. Locarnini, A. Mishonov, T. Boyer, H. Garcia, O. Baranova, D. Johnson, and D. Seidov (2013), World Ocean Atlas 2013, vol. 2: Salinity, NOAA Atlas NESDIS, 74, 39.